Numerical Computation of Hydrodynamic Wave Impact

Veldman, Arthur E.P.; Fekken, Geert; Kleefsman, K.M. Theresa

Published in:
EPRINTS-BOOK-TITLE

Publication date:
2005

Numerical Computation of Hydrodynamic Wave Impact

Arthur E.P. Veldman, Geert Fekken and K.M. Theresa Kleefsman
Institute of Mathematics and Computing Science
University of Groningen
PO Box 800, 9700AV Groningen, The Netherlands

veldman@math.rug.nl

ABSTRACT

Extreme waves, their impact loading on floating structures and the resulting dynamic response of these structures have long been subjects that could only be studied with experimental methods. Nowadays, computational CFD tools can make a significant contribution to these highly nonlinear flow problems. The paper starts with a short overview of the most popular numerical methods to simulate hydrodynamic wave loading. Emphasis will be on methods based on the Navier-Stokes equations. In particular, the ComFLOW method is presented, which belongs to the VOF family of free-surface simulation methods. Several examples of hydrodynamic impact are shown. For all flow cases experimental data is available to validate the outcome of the calculations.

1 INTRODUCTION

In extreme wave conditions floating or moored structures undergo large motion amplitudes and there is a high probability of large quantities of water coming onto the deck of such structures. Such events are accompanied by sudden and extremely violent water motions ('green water') and in this way present a real hazard for both the well-being of the crew and the integrity of the structure [1]. Captain D. MacIntyre described this situation during 'The Battle of the Atlantic' [2]: *"Their hulls whipped and shuddered in the huge Atlantic seas... solid green water swept destructively along their decks... For hour after hour this process repeated itself. Damage mounted, hull plates splitting, boats being smashed, men swept overboard and delicate anti-submarine devices put out of order..."*

Figure 1: Damage and first repair of a window on the Varg FPSO.

Over the years, various incidents with serious damage have been reported. For instance, in January 2000 the living quarters on the bow of the Varg FPSO were hit by green water, resulting in the damage of a window at the second floor, and flooding the area behind it (Fig. 1). The vessel was out of operation for a number of days. Another well-documented example is wave impact damage to the bow of the Schiehallion FPSO in 1998, resulting in an evacuation of the personnel and expensive hull repairs including redesign [3].

Existing analysis methods of vessel motion in waves are not capable of predicting such events to an acceptable level of accuracy. These analysis techniques largely depend on the application of linear potential flow theory [4, 5]. The physical phenomena accompanying extreme events are highly nonlinear in relation to the occurring wave elevations, and require new methods as a basis for prediction of the behaviour of the vessel and the water flow.

Thus, the desire for simulating complex free-surface problems like slamming, sloshing, splashing and the green water phenomenon has been present for a long time (e.g. [6-8]). The mathematical model for complex water flow dates from the first half of the 19th century already, known as the Navier-Stokes equations. However, it is only for a decade that these field equations can be solved for large scale complex free-surface flow problems, thanks to the increase in computer power and novel numerical algorithms.

This is an important development; in the near future it should provide, besides model testing, an additional tool for design problems involving these types of flows. This numerical tool is relatively cheap (in comparison with the operational costs of a model basin), therefore it can be used in an early stage of the design process. Further, it provides more detailed data for pressures and the velocity field than model tests.

The paper will give an impression of the state-of-the art of hydrodynamical methods for describing the extremely nonlinear flow of water in the vicinity of a floating structure in waves. It begins with a short overview of the existing basic methods for complex free-surface flows. Thereafter, the potential is demonstrated of the in-house developed method ComFLOW, which is based on the VOF technique, originally designed by Hirt and Nichols [9]. Some improvements will be presented that aim to overcome the weak points of the VOF approach. A detailed description of ComFLOW can be found in [10-13]. The simulations are validated with experiments, such as a dambreak flow, a steep wave event and the water entry of a free-falling body.

2 METHODS FOR FREE-SURFACE FLOW

To treat dynamically changing, arbitrary liquid configurations a large amount of flexibility has to be present in the numerical approach. An important ingredient is a ‘bookkeeping’ system for tracking the position of the liquid and its free surface [14]. In the literature a number of approaches can be found, of which a short assessment will be given next. A subdivision into three types of methods will be made: fixed-grid methods, moving-grid methods and gridless methods.

2.1 Fixed-grid methods

Using a fixed (or Eulerian) grid to discretise the mathematical model greatly reduces the grid generation effort. However, because the grid is not adapted to the boundaries and free surface, special attention must be paid to capture the position of the free surface and to the implementation of boundary conditions. When an appropriate free-surface tracking/capturing method is used, like Marker-and-Cell (MAC), Volume of Fluid (VOF) or level set, these methods can handle large free-surface deformations, including fluid splitting and fluid merging.

MAC and VOF

The Marker-and-Cell (MAC) method is the 'father' of all free-surface flow methods [15], and makes use of massless particles to keep track of the liquid region. Accuracy requires a considerable amount of particles per grid cell, making the method computationally expensive, especially in 3D. A cheaper way is to apply only surface markers (for a sophisticated example see e.g. [16]), but now splitting and merging of the surface are difficult to handle.

The MAC follow up is the Volume-of-Fluid (VOF) method introduced by Hirt and Nichols [9]; it has gained considerable popularity. Here a discrete indicator (or color) fuction is used that corresponds to the cell volume occupied by fluid. Although the original version of the reconstruction and displacement algorithm leads to considerable 'flotsam' and 'jetsam', i.e. artificial drops that numerically pinch off, variants can be designed that can track an arbitrarily moving free surface with high reliability [17,18]. A powerful variant is the piecewise linear reconstruction method (PLIC) introduced by Youngs [19]. Another successful member of this family is the CIP method [20]. An important property of VOF-type methods, resulting from its finite-volume philosophy, is the exact conservation of the amount of liquid present. Various maritime applications of VOF can be mentioned, e.g. [21-25].

Level set

An alternative to the indicator-function methods is the level set method [26], which makes use of a function representing the distance to the liquid surface. Reconstruction of the free surface is conceptually simpler than with the VOF method. However, for violently moving free surfaces the level set function requires to be redefined regularly, and conservation of the amount of liquid cannot be guaranteed [27]. Therefore, level set applications mainly focus on relative calm flows like the steady wave field around ship hulls [28-30], or above a submerged hydrofoil [31, 32]. To reduce mass loss, the level set method is sometimes combined with the VOF method [33].

2.2 Moving-grid methods

In moving-grid methods, also known as ALE (Arbitrary Lagrangian Eulerian) methods [34], each time step the grid is fitted to the moving free surface in a Lagrangian manner. Their advantage is that the boundaries are well defined, making it easy to apply boundary conditions; see e.g. [35]. However, when the free surface undergoes large deformation, splits or merges, these methods suffer great problems. This makes them less suitable for applications involving complex free-surface flows.

2.3 Gridless methods

Gridless methods represent the fluid by a large number of particles. In principle this makes them good methods for problems with large free surface deformations, fluid splitting and fluid merging. The smoothed particle hydrodynamics (SPH) method is an example of such a gridless method. It has first been applied to free-surface flows by Monaghan in an astrophysical context [36]. Later applications of SPH and similar methods include the splashing of breaking waves [37, 38], the dam breaking problem [39-41], and the response of floating structures [42]. The application of SPH to fluid dynamics is very young and the method is quite different from other methods, therefore little is known about appropriate numerical boundary conditions (e.g. non-reflecting conditions) and required computational effort (which is still very large because many particles and small time steps should be used).

3 MATHEMATICAL MODEL

3.1 Conservation of mass and momentum

Flow of a homogeneous, incompressible, viscous fluid is described by the continuity equation and the Navier-Stokes equations, describing conservation of mass and momentum, respectively. In a conservative form these are given by

$$\int_{\partial V} \mathbf{u}\cdot\mathbf{n}\, dS = 0, \quad \int_V \partial\, \mathbf{u}/\partial t\, dV + \int_{\partial V} \mathbf{u}\, \mathbf{u}^T\cdot\mathbf{n}\, dS = -1/\rho \int_{\partial V} (p\mathbf{n} - \mu\nabla\mathbf{u}\cdot\mathbf{n})\, dS + \int_V \mathbf{F}\, dV.$$

Here $\mathbf{u} = (u,v,w)$ denotes the velocity in the three coordinate directions, $\mathbf{n}$ is the normal at the boundary ∂V of the control volume V, ρ is the density, p is the pressure and ∇ is the gradient operator. Further, μ denotes the dynamic viscosity and $\mathbf{F} = (F_x, F_y, F_z)$ is an external body force like gravity.

3.2 Boundary conditions

At solid walls a no-slip boundary condition is used: $\mathbf{u} = 0$ for fixed boundaries, and $\mathbf{u} = \mathbf{u}_b$ for moving objects with $\mathbf{u}_b$ being the object velocity. When performing wave simulations an inflow boundary is needed where the incoming wave is prescribed, e.g. a regular linear wave or a 5th order Stokes wave. At the (opposite) outflow boundary a non-reflecting boundary condition is needed to prevent the waves from reflecting back into the domain. A Sommerfeld condition, e.g. [43], is appropriate in cases where a regular wave is used.

In the case of an irregular wave or a much deformed regular wave (e.g. due to the presence of an object in the flow) a damping zone can be added at the end of the domain (e.g. [44, 45]).

3.3 Free surface

When the position of the free surface is given by $s(\mathbf{x},t)=0$, its displacement of the free surface is described by the kinematic condition

$$Ds/Dt = \partial s/\partial t + (\mathbf{u}\cdot\nabla)s = 0.$$

At the free surface boundary conditions are necessary for pressure and velocity. Continuity of normal and tangential stress leads to the equations

$$p + 2\mu\, \partial u_n/\partial n = -p_0 + \sigma\kappa, \quad \mu\,(\partial u_n/\partial t + \partial u_t/\partial n) = 0.$$

Here, u_n and u_t are the normal and tangential component of the velocity respectively, p_0 is the atmospheric pressure, σ is the surface tension and κ denotes the total curvature of the free surface.

4 NUMERICAL MODEL—BASICS

4.1 Cartesian cut-cell method

To solve the Navier-Stokes equations numerically the computational domain is covered with a fixed Cartesian grid. The variables are staggered as in the original MAC method [15], which means that the velocities are defined on cell faces, whereas the pressure is defined in cell centres.

The body geometry is piecewise linear and cuts through the fixed rectangular grid: a cut-cell method (e.g. [46]). Volume apertures (F_b) and edge apertures (A^x, A^y and A^z) are used to indicate for every cell which

part of the cell and cell face, respectively, is open for fluid and which part is blocked. When moving bodies are present, these apertures are time dependent.

To track the free surface the Volume-of-Fluid function F_s is used, which is 0 when no fluid is present in the cell, 1 when the open part of the cell is completely filled with fluid and between 0 and 1 when the cell is partly filled with fluid. Cell labelling is introduced to distinguish between cells of different characters. First the cells that are completely blocked by geometry are called B(oundary) cells. These cells have volume aperture F_b=0. Then the cells that are empty but have the possibility of letting fluid flow in are labelled E(mpty). The adjacent cells containing fluid are S(urface) cells. The remaining cells are labelled as F(luid) cells. Note that these cells do not have to be completely filled with fluid. In Fig. 2 an example of the cell labelling is given.

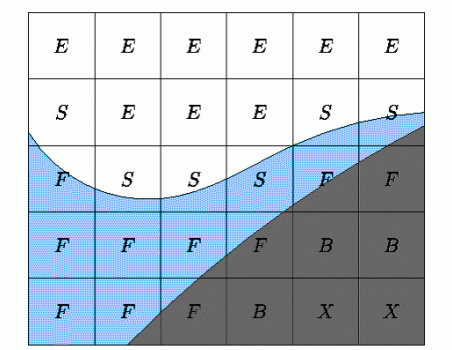

Figure 2: Cell labelling: dark grey denotes solid body, light blue is liquid

4.2 Discretisation of the continuity and momentum equations

The continuity and momentum equations are discretised using the finite volume method starting from the conservative formulation as given above.

The continuity equation is discretised in F-cells, taking the aperture information of the cut cells into account. The momentum equation is discretised at all faces between cells that contain fluid, i.e. at faces between F-cells and/or S-cells. For uncut cells as well as cut cells, the control volumes are defined as half of the open part of the left neighbour cell and half of the open part of the right neighbour cell. In this way, the centrally-discretized convection operator becomes skew-symmetric, as its analytical counterpart [47]. As a consequence, stability of the semi-discretized equations is guaranteed. Further, artificial diffusion is added such that it transfers the above central discretisation into a (more stable) first-order upwind discretisation.

For the diffusive term a discretisation is adopted in which the geometry is handled in a staircase way, so the cut cells are treated as if they are uncut. This has been done to prevent stability problems in small cut cells. In this way, the diffusive discretisation becomes first order, but in the convection-dominated simulations studied here diffusion is not really important [13].

The pressure gradient is discretised such that it becomes the negative transpose of the discrete divergence operator from the continuity equation, which is also an analytic property [47]. The external force is written as $F_g = -\nabla gz$, and it is discretised similar to the pressure gradient. In this way, it exactly cancels the discrete hydrodynamic pressure.

4.3 Time integration

The equations of motion are discretised in time using the forward Euler method. This first order method is accurate enough, because the order of the overall accuracy is already determined by the first order accuracy of the free-surface displacement algorithm. Using superscript n for the time level, the temporal discretisation results in

$$M^0\mathbf{u}^{n+1} = -M^b\mathbf{u}_b^{n+1}, \quad \Omega\,(\mathbf{u}^{n+1}-\mathbf{u}^n)/\delta t = -C\,(\mathbf{u}^n)\mathbf{u}^n - 1/\rho\,((M^0)^T p^{n+1} - \mu D\,\mathbf{u}^n) + \mathbf{F}^n.$$

The spatial discretisation is written in matrix notation, where M is the divergence operator with M^0 working on the interior velocities and M^b on the boundary velocities, Ω contains cell volumes, C contains the convective coefficients (which depend on the velocity vector) and D contains diffusive coefficients. Combining the above discrete equations a Poisson equation is obtained from which the pressure is solved [48]. It does not require boundary conditions at solid walls; at the free surface the boundary conditions follow from the normal-stress condition [15].

Numerical stability of the above time integration puts requirements on the maximum allowable time step, such as a CFL-condition.

More details about the discretisations described in this section are given in [10-13].

5 NUMERICAL MODEL—FREE-SURFACE ISSUES

This section describes some numerical issues concerning the treatment of the free surface: the displacement algorithm and the boundary conditions for the velocity. In particular with respect to these two issues adaptations to the original VOF method have been made.

5.1 Free-surface displacement

The free surface is displaced using an adapted version of the Volume-of-Fluid method from [9]. A piecewise constant reconstruction of the free surface is used, where the free surface is displaced by changing the VOF value in a cell using calculated fluxes through cell faces. The flux through a cell face is calculated as the velocity times the area of the cell face A and the time step δt: $\delta F^s = \mathbf{u}\cdot\mathbf{n}\,A\,\delta t$. Near the free surface these fluxes are constrained, based on available liquid and/or void space; we use the original flux expressions as given in [9].

The original VOF method has two main drawbacks. The first is that flotsam and jetsam can appear [17, 49], which are small droplets disconnecting from the free surface. The other drawback is the gain or loss of water due to rounding the VOF function when $F^s>1$ or $F^s<0$. By combining the VOF method with a local height function [11], these problems do not appear any more.

For every surface cell locally a function is defined that gives the height of the fluid in a column of three cells (Fig. 3). The direction in which the function is defined is the direction of the coordinate axis that is most normal to the free surface (the positive x-direction in Fig. 3}). Then, after calculating the fluxes across the cell boundaries of all three cells (the dashed-line region in Fig. 3) as in classical VOF, not the individual VOF values of the three column cells are updated, but the height function is updated. The individual VOF values of the three cells are then calculated from the height of the fluid in the column. When using this adapted fluid-displacement algorithm, the method is strictly mass conserving and almost no flotsam and jetsam appear.

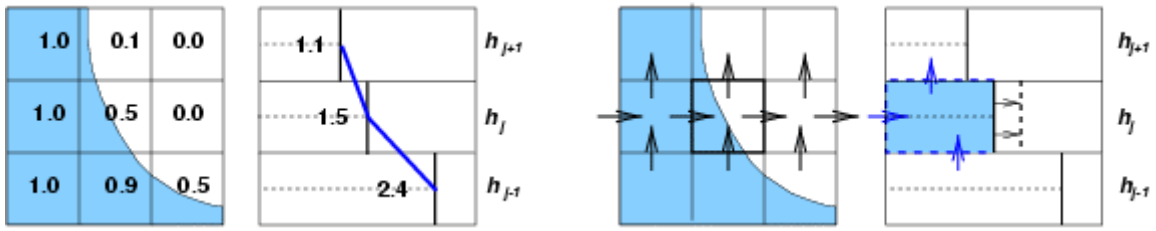

Figure 3: The VOF function in surface cells is updated using the local height function (left:definition of height function; right: update)

Both methods, the original VOF method and the VOF method combined with a local height function, have been compared in a dambreak simulation. In Fig. 4 (left) the result is shown of the free surface configuration of a calculation with the original VOF displacement method. The created flotsam and jetsam, small droplets disconnecting from the free surface, are clearly visible. When combining VOF with a local height function, the amount of flotsam and jetsam has decreased considerably as can be seen in Fig. 4 (right). In Fig. 5, the change of the total water volume during the dambreak simulations is shown. The loss of water using original VOF is considerable: about 7% after 6 seconds. In the adapted VOF method, the loss of water is only 0.02%, so mass is much better conserved.

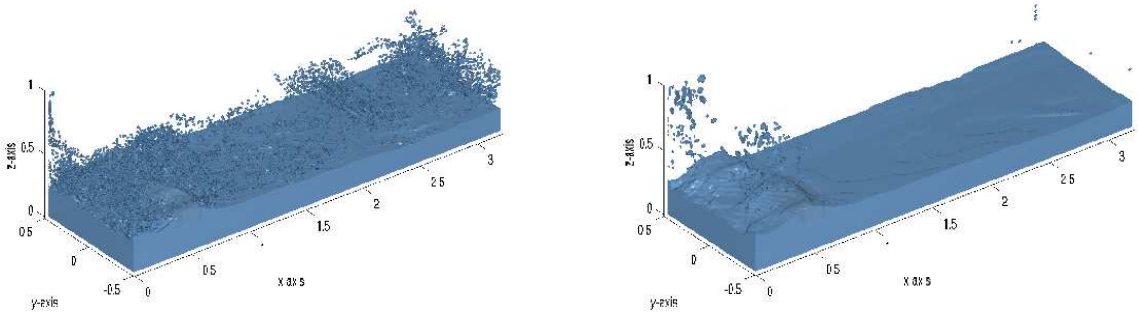

Figure 4: Snapshots at the end of dambreak flow simulations with different algorithms for the displacement of the free surface: original VOF (left) and VOF combined with a local height function (right).

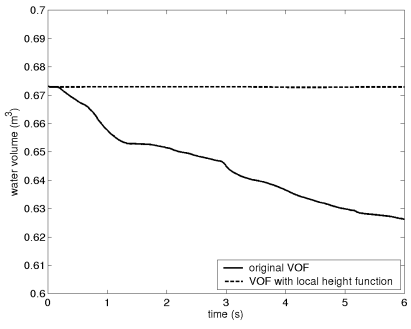

Figure 5: Change in water volume during a dambreak simulation using original VOF and VOF combined with a local height function.

5.2 Velocities near the free surface

Velocities in the neighbourhood of the free surface can be grouped in different classes (see Fig. 2). The first class contains the velocities between two F- and/or S-cells, which are determined from the momentum equation. The second class consists of the velocities between an S- and an E-cell. These velocities are determined using boundary conditions that will be described below. The third class consists of velocities between two E-cells that are needed to solve the momentum equation. These are determined using the tangential free-surface condition as described in [11].

Here we will focus on the velocities at the cell faces between S- and E-cells (SE-velocities), as their treatment turns out to have significant consequences for the robustness and the accuracy of the simulation method.

We discuss two methods, with their respective pro's and con's.

- *Method 1:* The divergence of every S-cell is set to zero as in original MAC [15]. In the case that only one SE-velocity is present in the S-cell, this velocity is uniquely defined. In the case that more E-cells surround the S-cell, the net mass flux through FS-boundaries is divided over the SE-boundaries such that $\nabla \cdot \mathbf{u}=0$ is satisfied.
- *Method 2:* The SE-velocities are determined by extrapolating interior velocities. The velocities used for the extrapolation are taken from the direction of the bulk of the fluid. Both constant and linear extrapolation are considered.

	accuracy wave	robustness	smooth p
$\nabla \cdot \mathbf{u}=0$	–	–	+
extrapolation	+	linear – constant +	–

Table 1: Summary of the performance of the two methods for SE-velocities.

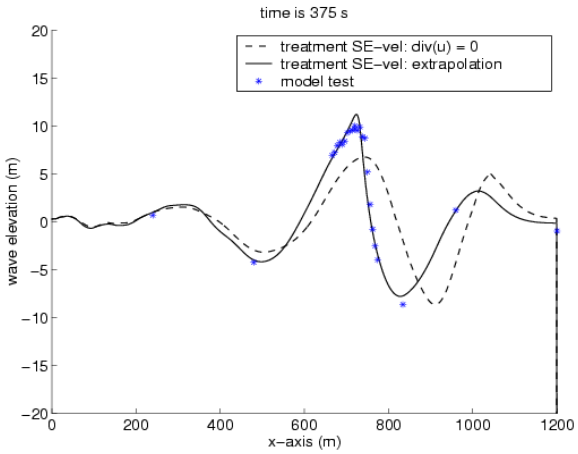

Figure 6: Different methods for free-surface velocities in a steep wave simulation: $\nabla \cdot u=0$ and linear extrapolation.

Table 1 summarises the performance of the methods with respect to accuracy, robustness and smoothness of the pressure field in wave simulations. The first column of Table 1 indicates that Method 1 gives less accurate results than Method 2. This difference can be seen in Fig. 6, where a snapshot of the wave elevation in a steep wave event is shown. Method 2, indicated by the solid line, gives a good prediction of the wave elevation compared to the measurements. The predicted elevation using Method 1 is worse: when using extrapolation from the interior velocity field the velocities are much better estimated than when using the criterion $\nabla\cdot\mathbf{u}=0$.

In the second column of Table 1 the robustness of the methods is indicated. The low robustness of Method 1 originates from instabilities in cut cells. E.g. in the situation as sketched in Fig. 7 the SE-velocity is calculated using

$$u_{SE} = (A^z_{SS}\, w_{SS} - A^x_{FS}\, u_{FS} - 0) / A^x_{SE}$$

to satisfy $\nabla\cdot\mathbf{u}=0$. Because of the large ratio between the SE-aperture and the other apertures, the SE-velocity will become very large. If this configuration is stationary during a number of consecutive time steps, the time integration will become unstable. Also the linear extrapolation method can lead to instabilities when the velocity field is not smooth. When using constant extrapolation, the method is much more robust

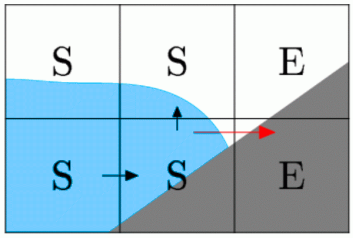

Figure 7: Very large SE-velocity when using Method 1.

The smoothness of the pressure field in the two methods is described in the third column of Table 1. When with Method 2 a surface (or empty) cell of which the divergence is not zero (i.e. $\nabla\cdot\mathbf{u} \neq 0$) changes into a fluid cell, the pressure has to respond within one time step to restore $\nabla\cdot\mathbf{u}=0$. This shows up as spikes in the pressure signal (see Fig. 12). By construction, these spikes do not appear in Method 1, where always $\nabla\cdot\mathbf{u} = 0$ in surface cells.

To overcome the problems described above, in practice a method is chosen that is an engineering mix between the two methods. The extrapolation method with constant extrapolation performs best and has been chosen in our numerical method. But to prevent spikes in the pressure signal, $\nabla\cdot\mathbf{u} = 0$ is enforced during each time step when a cell changes label from surface cell to fluid cell. The constant extrapolation is changed to linear extrapolation when greater accuracy in wave simulations is needed. This combination results in a highly accurate and very robust method.

Remark: In a two-phase computational model, everywhere in the domain the fluid velocity is calculated [50]. Aa a result the velocity will be smooth and moreover it is always divergence-free. Thus, the ambiguitiy in selecting conditions for the SE-velocities is circumvented, and the pressure signal is expected to be smooth. First experiences with such an approach do confirm these advantages of a two-phase approach [51].

5.3 Interactive body-fluid motion

In the current method the objects are either moving with a prescribed motion, or the motion is calculated from the interaction between the object and the liquid dynamics. Simulations with prescribed moving objects are only an approximation of reality, since the motion of the body usually is unknown, as it is affected by the forces the fluid exerts on the body [52]. In this section a full coupling between the liquid motion and the body motion is described.

The acceleration of the body can be computed by Newton's second law $A_{body} = I^{1} F_{body}$, where I is the inertia matrix and F_{body} contains the forces and moments exerted by the fluid. An explicit integration of Newton's second law, where the body motion follows from the forces exerted by the liquid ($A_{body}^{n+1} = I^{1} F_{body}^{n}$), is not guaranteed to be stable as we will show. When assuming a simple hydrodynamic model from added mass potential theory (one-dimensional, without rotations, hence $I=m$ with m the mass of the body), the force on the body can be calculated as $F_{body}= -m_a A$, with m_a being the added mass of the body. Inserting this into the explicit integration gives $A^{n+1} = -(m_a/m) A^{n}$. This system is only stable when $m_a/m \leq 1$. In other words, it is required that the mass of the moving body is larger than its added mass. For floating bodies this will not always be true, implying that this explicit integration cannot be used in that case.

To ensure stability in all cases, per time step an iterative method is used to, effectively, solve the problem fully implicit. In this sub-iteration underrelaxation can safely be applied to compensate the factor m_a/m without destroying temporal accuracy. For problems with moving bodies that are heavy, the coupling will be stable with just a bit underrelaxation. About 1-3 iteration steps are needed in that case. However, for lighter bodies more underrelaxation is needed. Typically, the number of sub-iterations is between 1 and 20, depending on the body mass and the magnitude of the fluid forces acting on the body. This slows down the method, because in every sub-iteration step the Poisson equation for the pressure has to be solved. However, the method is stable and performs well.

6 VALIDATION AND EXAMPLES

6.1 Dambreak simulation

At the Maritime Research Institute MARIN experiments have been performed with breaking dam flows. These experiments can be seen as a simple model of green water flow on the deck of a ship. The dambreak is a very popular validation case, because the set-up is easy: no special in- or outflow conditions are needed. A large tank of 3.22 by 1 by 1 meter is used with an open roof. The right part of the tank is closed by a door. Behind the door 0.55 meter of water is waiting to flow into the tank when the door is opened. In the tank a box has been placed that represents a scale model of a container on the deck of a ship.

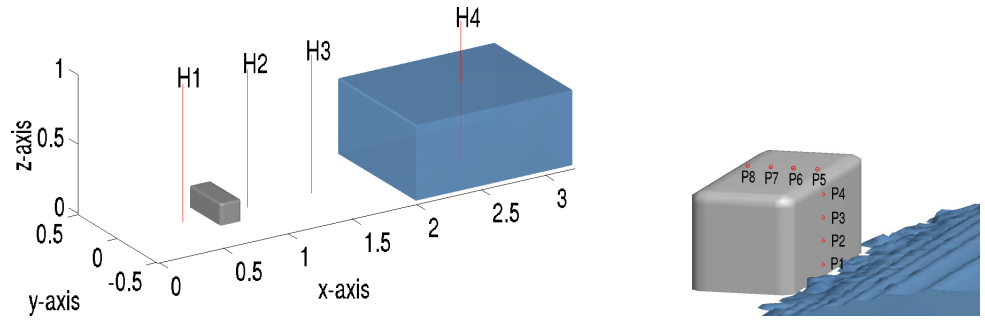

Figure 8: Measurement positions for water heights (left) and pressures (right) in the dambreak experiment.

During the experiment measurements have been performed of water heights, pressures and forces. In Fig. 8 the positions of the measured quantities are shown. Four vertical height probes have been used; one in the reservoir and the other three in the tank. The box was covered by eight pressure sensors, four on the front of the box and four on the top. The forces on the box were also measured.

As initial configuration of the simulation with ComFLOW, the water in the right part of the domain is at rest. When the simulation is started, the water starts to flow into the empty part of the tank. A fine grid of 236×76×68 grid cells has been used with some stretching towards the bottom of the tank. The simulation is continued for 6 seconds with an automatically adapted time step using maximum CFL-numbers around 0.75, resulting in a time step of the order of 0.001 seconds.

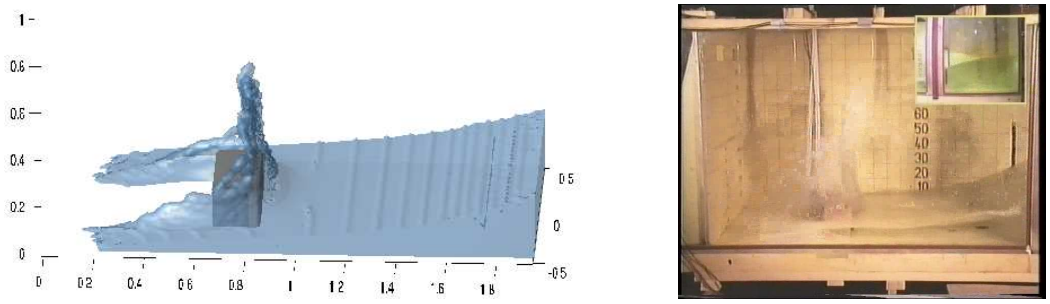

Figure 9: Snapshots of a dambreak simulation with a box in the flow compared with experiment at time 0.56 seconds

In Fig. 9 a snapshot of the early stage of the simulation is shown together with an image of the video from the experiment (at the same instant in time). There is a very good agreement between the snapshots of simulation and experiment. The time instant when the water is first hitting the box is the same. The shape of the free surface bending a bit forward is seen in both experiment and simulation. In the simulation the free surface has some ripples, which can be suppressed by using a piecewise linear reconstruction of the free surface [19] instead of the reconstruction aligned with the coordinate axes used in this study.

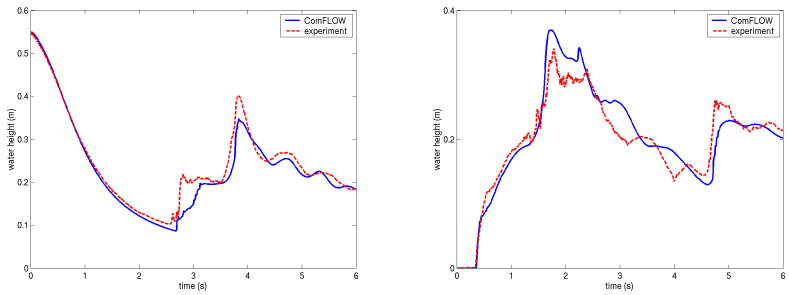

Figure 10: Vertical water heights in the reservoir at position H4 (left) and in the tank at H2 (right).

In Fig. 10 time histories of the water height at two locations are shown: in the reservoir, and in the tank just in front of the box. The agreement in both pictures is very good until the water has returned from the back wall (after about 1.8 seconds). After that some differences occur, but the global behaviour is still the same. After the water has returned from the wall, the fluid height at probe H2 is the largest. The water flows back to the reservoir, where it turns over again after about 4 seconds. The moment that this second wave meets the height probe at H2 again (after about 5 seconds) is almost exactly the same in simulation and experiment.

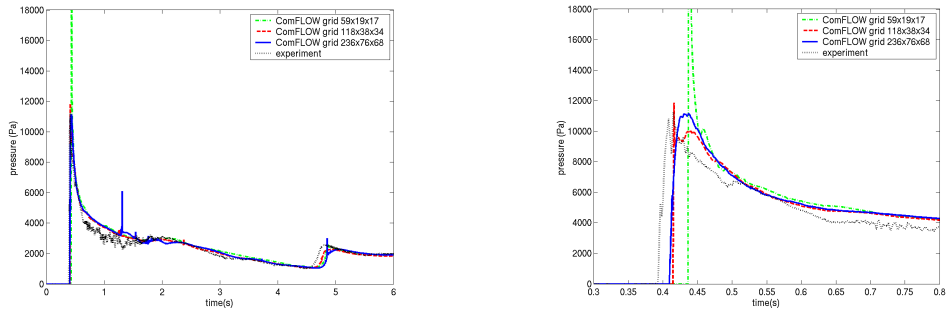

Figure 11: Pressure signals at the lower front of the box (P1) upon grid refinement; the right picture zooms in near first impact.

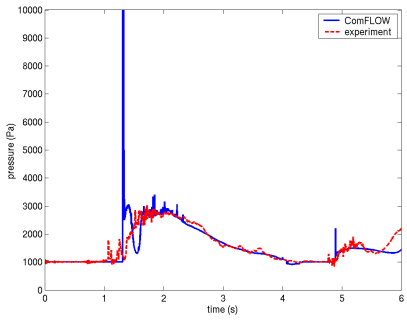

Figure 12: Pressure signal at the top of the box (P7).

The instant when the wave hits the box is perfectly captured by the simulation as can be seen from Figs. 11 and 12. Here the pressure at point P1 at the front of the box and P7 at the top of the box (see Fig. 8) are shown. In P1 (the lowest on the box) the magnitude of the impact pressure is the same for simulation and experiment. The moment the return wave hits the box again (after about 4.7 seconds) is visible in the graphs. In Fig. 12, where the pressure signal from sensor P7 at the top of the box is shown, a difference occurs between simulation and experiment. After about 1.3 seconds there is a wiggle in the simulation with duration of 0.5 seconds, which is not present in the experiment. Before this point the water hits the top of the box when the wave coming back from the wall is overturning.

Several spikes appear in the pressure signals that are visible in all the graphs at the same moment (for example at 1.3 seconds). These spikes occur because some water enters an empty cell that is completely surrounded by cells with fluid. When the water enters the E-cell, there is no empty cell left in the neighbourhood, so this cell changes to a fluid cell in one time step without being a surface cell in between. This discontinuous change in label and the corresponding restoration of $\nabla \cdot \mathbf{u}=0$, results in a pressure peak over the whole pressure field.

In Fig. 11 also a grid refinement study of the dambreak simulation is shown. Three different grids have been used with, in increasing order, 59×19×17, 118×38×34 and 236×76×68 grid points. The pressure along the lower part of the front side of the box is shown. The overall flow of the water is pretty much the same in all three grids, but when zooming in on the pressure peak (in the right picture) differences become visible. The coarsest grid is clearly not good enough. The pressure peak is over predicted and the water reaches the box too late. Although the water reaches the box earlier in the finer grids, there is still a small difference between simulation and experiment.

6.2 Green water shipping

In another experiment at MARIN, a more complex study of green water shipping on the deck of a moving FPSO vessel in high regular waves has been performed. For this validation study, measurements were carried out of the wave in front of the FPSO, and of water heights and pressures on the deck. The selected wave has a period of 12.9 seconds and the wave length is 260 meter, equal to the length of the FPSO. The wave amplitude is 6.76 meter. To be sure that the same wave has been used in the experiment and in the simulation, the wave measurement 230 meter in front of the bow of the vessel has been used to numerically initiate the wave at the inflow boundary. The motion of the ship has been prescribed using the measurements of the experiment. In Fig. 13 some snapshots of the simulation are shown. The large wave is building in front of the vessel after which it starts to flow onto the deck. The water flows off the deck when the ship is straightening.

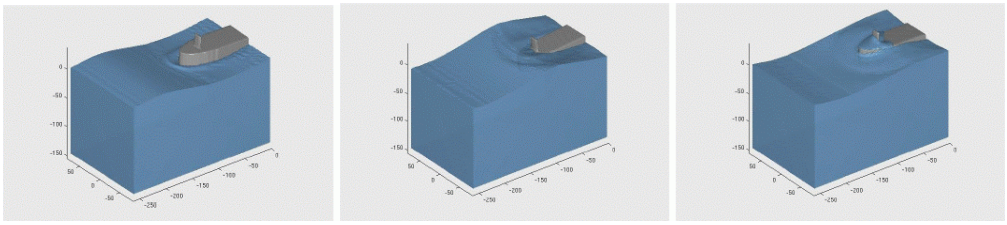

Figure 13: Snapshots of an FPSO shipping green water

The water height on the deck of the vessel has been compared in Fig. 14 (left). When the water has just flowed onto the deck, the agreement between the experiment and the simulation is reasonable. The moment in time the wave probe gets wet is almost the same. But in the first periods, the water height is somewhat higher in the simulation, whereas the total time the water hits the wave probe is shorter. Closer to the deck structure the total amount of water passing the wave probe is smaller in the simulation, but the velocity of the water on the deck is quite well predicted. A similar behaviour can be seen from the pressure on the deck (Fig. 14, right).

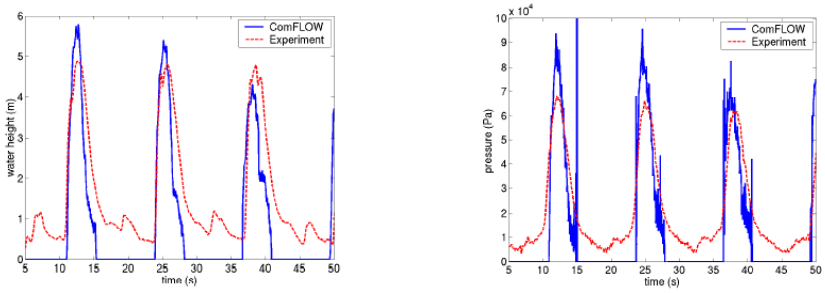

Figure 14: Water height (left) and pressure (right) on the deck of the FPSO: computation versus experiment.

6.3 Impact forces on a falling life-boat

Finally, we present a comparison that has been made with an experimental investigation of impact forces exerted on a falling life-boat (Fig. 15, left). A two-dimensional section of the life-boat has been used in the simulation (Fig. 15, right). The calculations have been performed in interactive mode, i.e. the motion of the life-boat follows from the interaction with the hydrodynamic forces (Section 5.3). Results are presented for a drop height of 3 meter. Forces on the life-boat have been calculated by measuring accelerations of the boat. The experimental data have been provided by Sastech BV [53]. Experimental and simulation results are shown in Fig. 16.

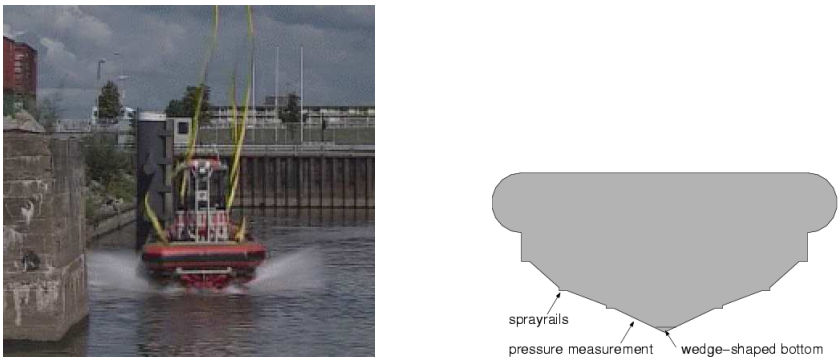

Figure 15: Snapshot of falling life-boat (left) and geometry of a two-dimensional section (right). The position of the pressure measurement is marked.

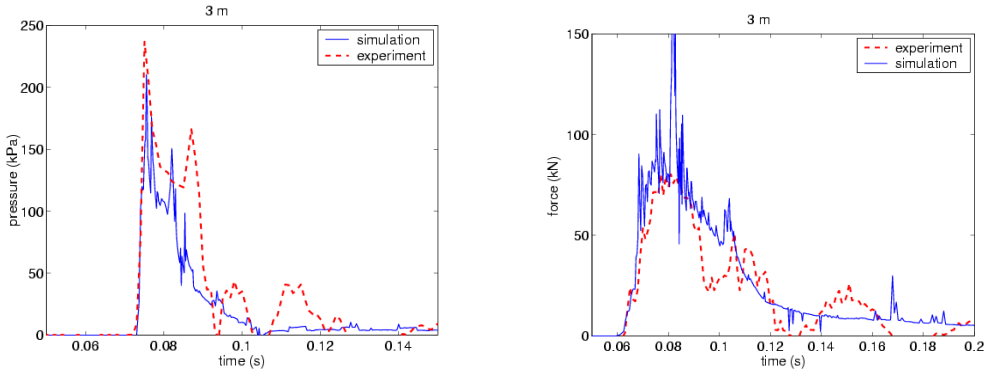

Figure 16: Experimental and simulation results for the falling life-boat with wedge-shaped bottom, dropped from 3 m. The left picture shows the pressure signal, the right picture shows the force signal.

It is found that the order of magnitude of the simulation results and the experimental results is quite similar. However, in the last stage of the signals, the experimental signals have a slightly oscillating pattern, which is not the case for the simulations. The effect of the sprayrails (the small horizontal pieces at the sloping edge of the life-boat, see Fig. 15 (right)) is remarkable. In the pressure signals, a secondary peak pressure is visible in both the experiments and the simulations ($t \approx 0.085$ sec). This is the effect of the first sprayrails. The forces of the simulation show a high peak force at the same time as the peak pressure, which is not visible in the experiments. The effect of the second sprayrails is clearly visible in the force signals of both the simulation and experimental results ($t \approx 0.1$ sec). In the pressure signals near the bottom of the boat the effect of these second sprayrails is hardly noticed: a consequence of the larger distance between the location of the second sprayrails and the location where the pressure is monitored.

7 CONCLUDING REMARKS

In the present paper results have been shown of the simulation of hydrodynamic impact problems using the Navier-Stokes solver ComFLOW. The finite volume discretisation with a cut-cell method on a fixed Cartesian grid results in a stable method, although the size of the fluid cells can get arbitrary small. The combination of the original VOF method with a local height function considerably improves the free-surface treatment by removing much of the flotsam and jetsam. Also, the sensitivity of the simulation results to the boundary conditions for the velocities at the free surface has been discussed. With a proper

choice, the method can accurately simulate steep waves and is very robust.

Engineering applications have been presented for a dambreak flow (emulating green water flow) and two water entry problems. In all cases experimental data were available for validation purposes. The dambreak simulation featured an on-deck box on which pressures and forces have been measured and calculated. The comparison with experiment was found very good. A simulation of green-water shipping shows the predictive capabilities in case of moving vessels. Finally, the falling life-boat concerned a test case for the interactive body motion. Again, a good comparison with experimental force measurements was found.

The results of the simulations give much confidence in the performance of the method. The method will be developed further in the coming years by extending it towards compressible two-phase flows. A major advantage of a two-phase model is that the boundary conditions for the velocities at the free surface, which have a large influence on the robustness and accuracy of the method, are not needed anymore. Also, in this way pockets of entrapped air in the wave impact region can be modelled; these can have a substantial influence on the impact pressures [54-56]. The method will also be extended with a coupling to an outer domain, where waves are generated using a computationally much cheaper potential flow diffraction code. In this way the Navier-Stokes domain can be limited to the close surroundings of the places of impact. For validation, simulations of a moving vessel in high waves resulting in green water on the deck will be performed and compared with experiments [57]. Besides green water and bow impact simulations, the focus will also be on sloshing, e.g. on board LNG tankers [51].

Acknowledgements

The paper describes the efforts of the ComFLOW development team at the University of Groningen, which operates in close cooperation with the Maritime Research Institute MARIN (The Netherlands) and FORCE Technology (Norway). In particular, the authors would like to acknowledge the contributions of their colleagues (in alphabetical order) Jeroen Gerrits, Erwin Loots, Roel Luppes and Rik Wemmenhove at the University of Groningen; Bas Buchner, Tim Bunnik and Arjan Voogt at MARIN; and Erik Falkenberg and Bogdan Iwanowski at FORCE Technology. Also, the authors are grateful to Frans Sas of SasTech (The Netherlands) for providing the experimental data of the falling life-boat.

Part of the research has been funded by MARIN. Another part has been carried out in the SAFE-FLOW project (SAFE-FLOating offshore structures under impact loading of shipped green water and Waves), funded by the European Community under the 'Competitive and Sustainable Growth' Programme (EU Project No.: GRD1-2000-25656) and a group of 26 industrial participants (oil companies, shipyards, engineering companies, regulating bodies). The authors are solely responsible for the present paper and it does not represent the opinion of the European Community.

References

[1] W.D.M. Morris, J. Millar, B. Buchner, Green water susceptibility of North Sea FPSO/FSUs, In: *Proc. 15th Conf. Floating Production Systems (FPS),* London, 2000.

[2] D. MacIntyre, *The Battle of the Atlantic*. Batsford, London, 1961.

[3] P. Gorf, N. Barltrop, B. Okan, T. Hodson, R. Rainey, FPSO bow damage in steep waves, *Proc. Rogue Waves,* Brest, 2000.

[4] B. Buchner, *Green water on ship-type offshore structures*. PhD thesis, Department of Maritime Technology, Delft University of Technology, 2002.

[5] R.W. Yeung, Numerical methods in free-surface flows. *Ann. Rev. Fluid Mech.* 12:395-442, 1982.

[6] W. Tsai and D.K.P. Yue, Computation of nonlinear free-surface flows. *Ann. Rev. Fluid Mech*. 28:249-278, 1996.

[7] O.M. Faltinsen, *Sea Loads on Ships and Offshore Structures.* Cambridge University Press, 1999.

[8] B. Molin and J. Ferziger, Hydrodynamique des structures offshore. *Appl. Mech. Rev.* 56:B29, 2003.

[9] C.W. Hirt and B.D. Nichols, Volume of fluid (vof) method for the dynamics of free boundaries. *J. Comp. Phys*. 39:201-225, 1981

[10] G. Fekken, *Numerical simulation of free-surface flow with moving rigid bodies.* PhD thesis, University of Groningen, 2004, URL http://www.ub.rug.nl/eldoc/dis/science/g.fekken.

[11] J. Gerrits, *Dynamics of liquid-filled spacecraft.* PhD thesis, Department of Mathematics, University of Groningen, 2001. URL http://www.ub.rug.nl/eldoc/dis/science/j.gerrits.

[12] J. Gerrits and A.E.P. Veldman, Dynamics of liquid-filled spacecraft. *J. Eng. Math*. 45:21-38, 2003.

[13] K.M.T. Kleefsman, G. Fekken, A.E.P. Veldman, B. Iwanowski, and B. Buchner, A Volume-of-Fluid based simulation methods for wave impact problems. *J. Comput. Phys*. 206:363-393, 2005.

[14] R. Scardovelli, S. Zaleski. Direct numerical simulation of free-surface and interfacial flow*, Ann. Rev. Fluid Mech*. 31, 567-603, 1999.

[15] F.H. Harlow and J.E. Welch, Numerical calculation of time-dependent viscous incompressible flow of fluid with free surface. *Phys. Fluids* 8:2182-2189, 1965.

[16] D. Juric and G. Tryggvason, A front tracking method for dendritic solidification. *J. Comput. Phys*. 123:127-148, 1996.

[17] W.J. Rider and D.B. Kothe, Reconstructing volume tracking. *J. Comput. Phys*. 141:112-152, 1998.

[18] M. Rudman, Volume-tracking methods for interfacial flow calculations. *Int. J. Numer. Methods Fluids* 24:671-691, 1997.

[19] D.L. Youngs, *An interface tracking method for a 3D Eulerian hydrodynamics code*, Technical Report AWRE/44/92/35, Atomic Weapons Research Establishment, 1987.

[20] T. Yabe, F. Xiao and T. Utsumi, The constrained interpolation profile method for multiphase analysis. *J. Comp. Phys*. 169:556-593, 2001.

[21] A. Cariou and G. Casella, Liquid sloshing in ship tanks: a comparative study of numerical simulation. *Marine Structures* 12:183-198, 1999.

[22] M. Greco, O.M. Faltinsen and M. Landrini, Numerical simulation of heavy water shipping. In: *Proc. 17th Workshop on Water Waves and Floating Bodies*, Cambridge UK, 14-16 April 2002.

[23] Y. Kim. Numerical simulation of sloshing flows with impact load. *Applied Ocean Research* 23:53-62, 2001.

[24] S. Muzaferija, M. Peric, P. Sames and T. Schellin, A two-fluid Navier-Stokes solver to simulate water entry. In: *Proc. 22nd Symp. on Naval Hydrodynamics*, pp. 638-649, 2001.

[25] T. Sarkar, Application of a RANS technique for simulation of the flow past a body in heaving and rolling motions at the free surface. In: *Proc. MARNET - CFD First Annual Workshop*, Barcelona, 18-19 November 1999.

[26] J.A. Sethian, *Level Set Methods: Evolving Interfaces in Geometry, Fluid Mechanics, Computer Vision and Materials Science.* Cambridge University Press, 1996.

[27] W.J. Rider and D.B. Kothe, Stretching and tearing interface tracking methods. *AIAA paper 95-1717*, 1995.

[28] D. Dommermuth, G. Innis, T. Luth, and E. Novikov, Numerical simulation of bow waves. In: *Proc. 22th Symp. Naval Hydrodynamics*, page 159, 1998.

[29] M. Sussman and D. Dommermuth, The numerical simulation of ship waves using cartesian grid methods. In: *Proc. 23th Symp. Naval Hydrodynamics*, pp. 762-779, 2001.

[30] H.H. Chun, I.R. Park, and S.K. Lee, Analysis of turbulent free-surface flow around hulls in shallow water channel by a level-set method. In: *Proc. 23th Symp. Naval Hydrodynamics*, pp. 941-956, 2001.

[31] A. Iafrati, A. Olivieri, F. Pistani, and E. Campana, Numerical and experimental study of the wave breaking generated by a submerged hydrofoil. In: *Proc. 23th Symp. Naval Hydrodynamics*, pp. 746-761, 2001.

[32] M. Vogt. *A comparison between moving grid and a level set technique for solving 2d free surface flows.* Technical Report CHA/NAV/R-98/0054, Chalmers University, 1998.

[33] M. Sussman and E.G. Puckett, A coupled level set and volume-of-fluid method for computing 3d and axisymmetric incompressible two-phase flows. *J. Comput. Phys*. 162:301-337, 2000.

[34] C.W. Hirt, A.A. Amsden, J.L. Cook, An arbitrary Lagrangian-Eulerian method for all flow speeds. *J. Comutp. Phys.* 14:227-253, 1974.

[35] B. Alessandrini and G. Delhommeau, A fully coupled Navier-Stokes solver for calculation of turbulent incompressible free surface flow past a ship hull. *Int. J. Num. Meth. Fluids* 29:125-142, 1999.

[36] J.J. Monaghan, Smoothed Particle Hydrodynamics. *Ann. Rev. Astron. Astrophys*. 30:543-74, 1992.

[37] E. Fontaine, M. Landrini, and M.P. Tulin, On modeling the post breaking phase: Splashing. In: T. Miloh and G. Zilman (eds.) *Proc. 15th Int. Workshop Water Waves and Floating Bodies*, 2000.

[38] M.P. Tulin and M. Landrini, Breaking waves in the ocean and around ships. In: *Proc. 23th Symp. Naval Hydrodynamics*, pp. 713-745, 2001.

[39] J.J. Monaghan, Simulating free surface flows with SPH. *J. Comp. Phys*. 110:399-406, 1994.

[40] Y. Andrillon, M. Doring, B. Alessandrini, and P. Ferrant, Comparison between sph and vof free surface flow simulation. In: *Proc. 5th Numerical Towing Tank Symposium*, 2002.

[41] A. Colagrossi and M. Landrini, Numerical simulations of 2-phase flows by smoothed particle hydrodynamics. In: *Proc. 5th Numerical Towing Tank Symposium*, 2002.

[42] H. Maeda, K. Nishimoto, K. Masuda, T. Asanuma, M.M. Tsukamoto, and T. Ikoma, Numerical analysis for hydrodynamic motions of floating structure using MPS method. In: *Proc. 23rd Int. Conf. on Offshore Mechanics and Arctic Engineering OMEAE2004*, June 20-25, Vancouver, 2004.

[43] I. Orlanski, A simple boundary condition for unbounded hyperbolic flows, *J. Comput. Phys*. 21:251-269, 1976.

[44] A. Clément, Coupling of two absorbing boundary conditions for 2D time-domain simulations of free surface gravity waves, *J. Comput. Phys*. 126:139-151, 1996.

[45] M. Israeli, S.A. Orszag, Approximation of radiation boundary conditions, *J. Comput. Phys*. 41:115-135, 1981.

[46] G. Yang, D.M. Causon and D.M. Ingram, Calculation of compressible flows about complex moving geometries using a Cartesian cut cell method. *Int. J. Num. Meth. Fluids* 33:1121-1151, 2000.

[47] R.W.C.P. Verstappen and A.E.P. Veldman, Symmetry-preserving discretisation of turbulent flow. *J. Comput. Phys.* 187:343-368, 2003.

[48] E.F.F. Botta, M.H.M. Ellenbroek, A Modified SOR Method for the Poisson Equation in Unsteady Free-Surface Flow Calculations, *J. Comput. Phys*. 60:119-134, 1985.

[49] D.J.E. Harvie, D.F. Fletcher, A new volume of fluid advection algorithm: the stream scheme, *J. Comput. Phys*. 162:1-32, 2000.

[50] S.J. Osher and G. Tryggvason (eds.) Special issue on `Computational methods for multiphase flows'. *J. Comput. Phys*. 169:249-759, 2001.

[51] R. Wemmenhove, E. Loots, R. Luppes, A.E.P. Veldman. Modelling two-phase flow with offshore applications. In: *Proc. 24th Int. Conf. on Offshore Mechanics and Arctic Engineering*, Halkidiki, Greece, paper OMAE2005-67460, 2005.

[52] P. Ferrant, Simulation of strongly nonlinear wave generation and wave-body interactions using a 3D MEL model. In: *Proc. 21st Symp. Naval Hydrodynamics*, pp. 93-109, 1997.

[53] F. Sas, Private communication, 2003.

[54] D.H. Peregrine and L. Thais. The effect of entrained air in violent water wave impacts. *J. Fluid Mech*. 325:377-397, 1996.

[55] D.J. Wood, D.H. Peregrine and T. Bruce. Wave impact on a wall using pressure-impulse theory. *J. Waterway, Port, Coastal and Ocean Engng*. 126:182-190, 2000.

[56] J.H. Duncan, Spilling breakers. *Ann. Rev. Fluid Mech*. 33:519-547, 2001.

[57] K.M.T. Kleefsman, E. Loots, A.E.P. Veldman, B. Buchner, T.H.J. Bunnik, and E. Falkenberg, The numerical simulation of green water loading including vessel motions. In: *Proc. 24th Int. Conf. on Offshore Mechanics and Arctic Engineering*, Halkidiki, Greece, paper OMAE2005-67448, 2005.